Available online at www.sciencedirect.com

ScienceDirect

Procedia CIRP 74 (2018) 196–200

www.elsevier.com/locate/procedia

10th CIRP Conference on Photonic Technologies [LANE 2018]

Laser additive manufacturing of oxide dispersion strengthened steels using laser-generated nanoparticle-metal composite powders

Markus B. Wilms[a], René Streubel[b], Felix Frömel[c], Andreas Weisheit[a], Jochen Tenkamp[c], Frank Walther[c], Stephan Barcikowski[b], Johannes Henrich Schleifenbaum[a], Bilal Gökce[b,*]

[a]*Chair for Digital Additive Production (DAP), RWTH Aachen University and Fraunhofer Institue of Laser Technology (ILT), 52074 Aachen, Germany*

[b]*Technical Chemistry I and Center for Nanointegration Duisburg-Essen (CENIDE), University Duisburg-Essen, 45141 Essen, Germany*

[c] *TU Dortmund University, Department of Materials Test Engineering (WPT), Baroper Str. 303, D-44227 Dortmund, Germany*

* Corresponding author. Tel.: +49-201-183-3146; fax: +49-201-183-3049. *E-mail address:* bilal.goekce@uni-due.de

Abstract

A new route for the synthesis of powder composites suitable for processing with laser additive manufacturing is demonstrated. The powder composites, consisting of micrometer-sized stainless steel powder, homogenously decorated with nano-scaled Y_2O_3 powder particles, are manufactured by laser processing of colloids and electrostatic deposition. Consolidated by laser metal deposition and selective laser melting, the resulting specimens show superior mechanical properties at elevated temperatures, caused by the nano-sized, homogenously distributed dispersoids.

Keywords: Oxide dispersion strengthened materials; ODS; Laser additive manufacturing; Pulsed laser ablation in liquids; Selective Laser Melting

1. Introduction

Oxide dispersion steels are a promising structural material class for GenIV nuclear reactors as well as future fusion reactors [1, 2]. This material class is typically composed of a ferritic/martensitic steel matrix, alloyed with high amounts of chromium (9-20%) to exhibit corrosion resistance. The steel matrix is additionally reinforced with nanometer-sized dispersoids, composed of titanium-containing yttrium-based oxides [3,4], exhibiting low solubility in the steel matrix offering only low potential for coarsening by Ostwald ripening [5]. The homogeneously distributed dispersoids increase material strength in particular at high temperatures, such as creep resistance [8,9]. Additionally, they act as sinks for defects, induced by high-energy neutron or ion irradiation, and therefore increase the resistance against macroscopic material degradation, such as swelling [10-12].

The main fabrication route for ODS steels is the powder metallurgy route, consisting of a long-term (up to 48h), batch-wise mechanical alloying process that uses metal matrix alloy powder and a nanometer-sized yttrium oxide powder [13-15]. By ball milling in planetary or high-energy attritor type mills powder composites of metal and oxide particles are formed. This process is characterized by the dissolution of oxide particles into the metal powders, since the peak of yttrium oxide in XRD disappears with prolonged milling times [16]. The ball milling process is subsequently followed by various types of consolidation processes, such as hot-isostatic pressing or hot extrusion as well as various thermomechanical treatments in order to adjust the final microstructure of the alloy. The complex and expensive fabrication route for ODS

10.1016/j.procir.2018.08.093

steels still poses the main drawback for widespread industrial applications of these type of materials. Also, conventional techniques do not offer the possibility of near net shaped manufacturing. An alternative manufacturing method is Laser Additive Manufacturing (LAM), which is principally capable of producing ODS materials by offering high solidification rates in combination with strong Maragoni forces within small scaled melt pools. The principal capability of the LAM processes Laser Metal Deposition (LMD) [17] and Selective Laser Melting (SLM) [18-20] to produce ODS materials has been showed in various studies. However, in all cases mechanically alloyed powder has been utilized. In this study the feasibility of nanoparticle-metal powder composites, fabricated by a new route consisting of laser processing of colloids (LPC) and subsequent adsorption by pH-controlled electrostatic interaction on steel powders [21] for the LAM production of ODS materials is demonstrated. Mechanical characterization is performed by compression tests of specimens manufactured by LMD [22]. Additionally the powder was used to manufacture bulk specimens via SLM.

2. Materials and Methods

Ferritic, stainless steel powder (Nanoval) consisting of 21.03 wt% Cr, 4.67 wt% Al and 0.47 wt% Ti and with two powder particle fractions of < 45 µm for SLM and 45-90 µm for LMD was used for laser-based processing of colloids with 0.3 wt% commercial Y_2O_3 nanopowder (Sigma Aldrich).

2.1 Production of composite powders

A 10 ps laser (EdgeWave) with a wavelength of 355 nm was used with a laser power of 20 W and a repetition rate of 80 kHz to deagglomerate dispersed Y_2O_3 nanoparticles in an aqueous solution by laser processing of colloids (LPC) [23,24] via a flow jet configuration [25,26] (Fig. 1) for five passage cycles. The nanoparticles are adsorbed via electrostatic interaction by adjusting the pH value of the aqueous solution [25].

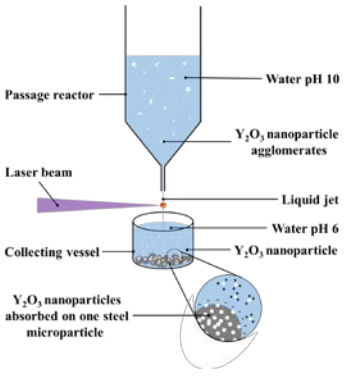

Fig. 1 Schematic drawing of the LPC process and the electrostatic deposition process in aqueous suspension

2.2 Consolidation via LAM

LMD is conducted on a three-axis handling system (Schuler-Held) equipped with a diode laser system (Laserline LDF 2000-30) emitting at wavelengths of 1025 and 1064 nm. Using a special optical setup a focal spot diameter of approx. 0.6 mm is generated. The powder is injected via a coaxial powder feed nozzle (Fraunhofer ILT) and a disc-based feeding system (GTV Verschleißschutz PF2/2) using Ar gas. Argon is fed through the beam path for additional shielding from the surrounding atmosphere.

Bulk samples were produced using a laser power of 370 W, a deposition speed of 2,000 mm/min and a powder feed rate of 1.3 g/min on a water-cooled plate to ensure rapid heat transfer to the substrate. A two directional deposition pattern, maintaining constant track offset of 350 µm and height offset of 210 µm, is used to manufacture bulk samples with 40 layers.

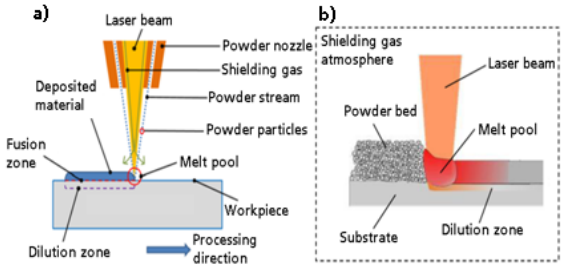

Fig. 2 Schematic drawing of LMD (left) and SLM (right)

SLM is conducted on a laboratory SLM machine (Aconity MIDI) equipped with a 1kW fiber laser (IPG YLR-1000-WC-Y14) emitting a wavelength of 1070 nm. The laser scanner is used to generate a focal spot diameter of approx. 80 µm. Cubic bulk samples (5 mm^3) were manufactured using a chess-like pattern with a constant layer height of 30 µm, a scanning speed of 800 mm/s and a laser power of 160 W.

2.3 Microstructural characterization

Microstructural characterization is conducted using light optical microscopy (LOM) after standard metallographic preparation of cross sections perpendicular to building direction and etching with “Nital” agent (3 Vol.% HNO_3 (aq.)). Additionally the samples are examined using a scanning electron microscope (Zeiss Leo 1455EP) in SE-mode.

2.4 Mechanical characterization

For mechanical characterization quasistatic compression tests with constant speed (v_c = 0.0833 mm/min) at room temperature and at 600°C were performed. A servohydraulic testing system (Schenck PC63M, Instron 8800 controller) with a 63kN load cell, equipped with a high temperature furnace (MTS 653) was used to test cylindrical water-jet cut specimens (diameter 4 mm, height 5-6 mm). Lubrication agent (Molykote) was used to minimize friction between the specimens and the compression dies.

3. Results

The laser processing (dispersion) of colloidal aqueous suspension of Y_2O_3 nanoparticles resulted in a significant reduction of the agglomerates (Fig. 3).
Figures 3a-c) show the presence of agglomerated Y_2O_3 nanoparticles in dependence of the used treatment method as imaged by SEM. While ultrasonication of the suspension already leads to deagglomeration, dispersion by means of LPC evidently leads to less agglomerates.

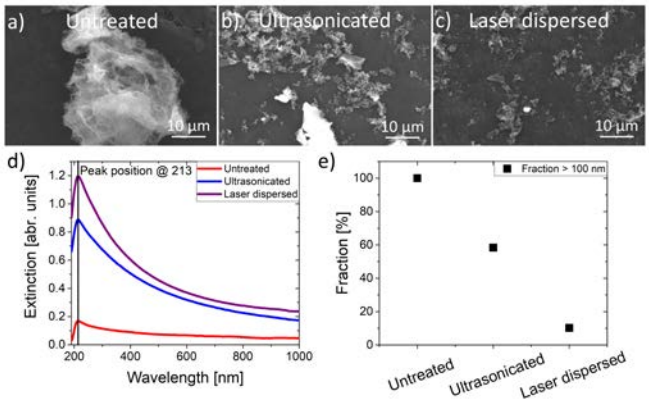

Fig.3 Deagglomeration of Y_2O_3 nanoparticles by different treatment methods. (a-c) SEM images. (D) UV-Vis extinction spectra. (E) Measurement of the fraction of Y_2O_3 nanoparticles with hydrodynamic diameters >100nm by dynamic light scattering.

This conclusion is also supported by UV-Vis extinction spectroscopy (Fig. 3d)) where the extinction is increased by a better dispersion of the nanoparticles (at the same concentration). Fig. 3e shows the fraction of particles larger than 100 nm for different dispersion methods as extracted from dynamic light scattering measurements. This method which is dominated by large scatting entities additionally supports the above observation, i.e., only laser dispersion by LPC leads to a significant reduction of the agglomerates.
The subsequent adsorption of laser-irradiated nanoparticles on raw steel powder, which is also performed in aqueous suspension, results in homogeneous distribution of nanoparticles on the steel raw powders surface (Fig. 4).

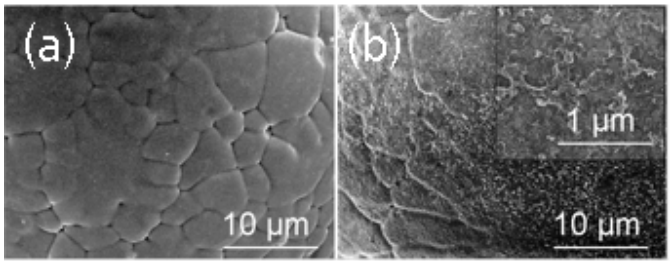

Fig.4 SEM image of raw steel powder (a) and decorated steel powder with 0.3wt% Y_2O_3 (b)

The nanoparticle deposition is achieved by dielectrophoretic interaction between nanoparticle and micropowder. For the suspension a pH of 6 is adjusted leading to negatively charged steel powder particles and positively charged nanoparticles. After deposition the suspension is dried in a furnace (50°C) for several hours. The steel powder does not additionally oxidize during its transient immersion time in water as confirmed by REM-EDX analysis.

The manufactured powder composites are processed with LMD with the setup described in 2.2. In contrast to non-reinforced steel powder the melt pool during processing becomes more turbulent, which is also indicated by increased spark formation. However, specimens with porosities of approx. 0.5% could be manufactured and no further adjustments of process parameters had to be performed. No cracks could be observed in the manufactured specimens. The microstructure is characterized by large elongated grains, which exceed the distance between interlayer boundaries and therefore indicate epitaxial grain growth (Fig. 5). The grains are oriented in building direction with a subtle inclination of a few degrees caused the curvature of the solidification front in combination with the used building strategy. Grain refinement by heterogeneous nucleation on dispersed nanoparticles is not observed. This may be related to the poor wettability of yttrium oxide by iron-chromium melts. Vickers hardness measurements (HV10) further confirm that (within the error of the measurement) the distributed nano-scaled oxides have no influence on hardness of the material (data not shown).

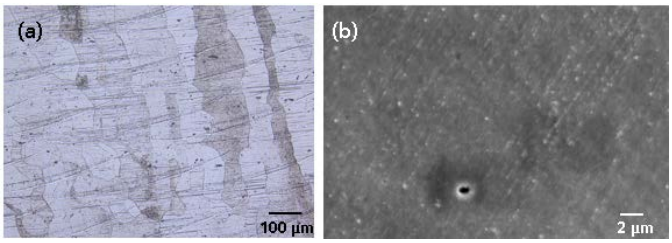

Fig.5 Light optical microscope image (a) of the microstructure of LMD produced sample, (b) SEM image revealing the presence of homogenously distributed oxide particles

A more critical test for ODS steels are compression tests at high temperatures, since these materials are typically used in high-temperature environments. The performed compression tests reveal decreasing mechanical strength with increasing testing temperature, which is expected and typical for steels. However, the mechanical properties of steel, reinforced with nano-scaled Y_2O_3 (labelled in Fig. 6 as "Y_2O_3"), are superior compared to the unreinforced material. Whereas the increase of compression stress at room temperature for reinforced steel is rather small, the increase at higher testing temperatures (600°C) becomes significantly more pronounced, which can be explained by impairment of climb or glide motion of dislocations by dispersed nanoparticles.

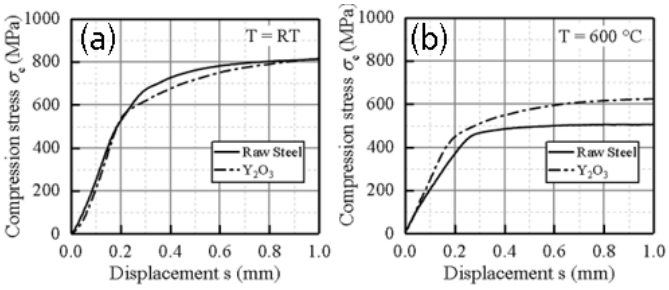

Fig.6 Averaged compression behavior at room temperature (a) and 600°C (b)

To test the SLM-processability of the powder composites, further specimens are built by SLM (Fig. 7). These specimens exhibit porosities of approx. 0.8%. The microstructure is characterized by elongated grains in building direction. The width of these grains is considerably smaller than the grains observed in LMD specimens, which may be caused by the utility of a smaller beam diameter and therefore higher solidification rates. Additionally, no inclination of the growth direction of the grains is visible. However, epitaxial grain growth can be observed.

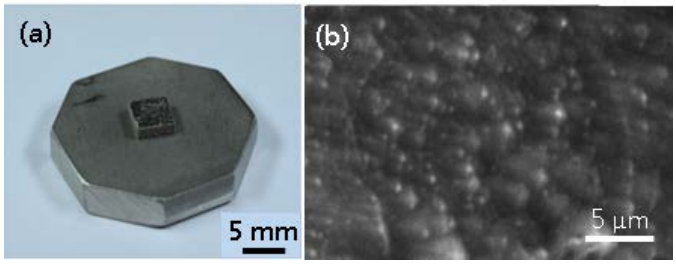

Fig. 7 Photograph of the SLM specimen on a 316L substrate material (a), SEM image of homogenously distributed oxides in SLM built specimen (b)

A large number of "spots" indicate the presence of sub-100 nm-sized dispersoids (Fig. 7 right). These small populations of dispersoids cannot be resolved by the resolution of the used SEM system. Detailed analysis of these areas require transmission electron microscopy but are not within the scope of this study.

4. Conclusions and Outlook

The feasibility of a novel powder synthesis route, consisting of LPC and subsequent electrophoretic deposition is demonstrated in this study. Powder composites, which are characterized by a homogenous distribution of Y_2O_3-nanoparticles on the surface of micrometer-sized stainless steel particles, could be synthesized. The powder composites were successfully processed by the two LAM processes of LMD and SLM, leading to bulk specimens with low porosities and homogenous distribution of nanoscale dispersoids. Compression tests at elevated temperatures demonstrate the superior performance of reinforced material compared to raw stainless steel specimens.
Future investigations will focus on the mechanical characterization of the SLM processed material as well as the microstructural characterization by TEM. In order to qualify these materials for industrial application further mechanical tests such as long-term creep tests and evaluation of high energy neutron resistance need to be performed.

Acknowledgments

We thank Veronica Rocio Molina Ramirez for conducting SEM analysis and Mareen Goßling for her contribution in performing SLM experiments.

References

[1] Odette GR, Alinger MJ, Wirth BD. Recent Developments in irradiation-resistant steels. Annu. Rev. Mater. Res. 2008;38:471-503.
[2] Ukai S, Fujiwara M. Perspective of ODS alloys application in nuclear environments. J. Nucl. Mater. 2002; 307-311: 749-757
[3] El-Genk M, Tournier J-M. A review of refractory metal alloys and mechanically alloyed oxide dispersion strengthened steels for space nuclear power systems. J. Nucl. Mater. 2005; 340: 93-112
[4] Ratti M, Leuvrey D, Mathon MH, de Carlan Y. Influence of titanium on nano-cluster (Y, Ti, O) stability in ODS ferritic materials. J. Nucl. Mater. 2009; 386-388: 540-543
[5] Knipling KE, Baker BW, Schreiber DK. Mechanisms of particle coarsening and phase transformation in oxide dispersion strengthened steels during friction stir welding. Microsc. Mircoa. 2016; 22; S3:676-677
[6] Wasilkowska A, Bartsch M, Messerschmidt U, Herzog R, Czyrska-Filemonowicz A. Creep mechanisms of ferritic oxide dispersion strengthened alloys. J. Mater. Proc. Tec. 2003; 133; 1-2: 218-224
[7] Susila P, Sturm D, Heilmaier M, Murty BS, Subramanya Sarma V. Effect of yttria particle size on the microstructure and compression creep properties of nanostructured oxide dispersion strengthened ferritic (Fe-12Cr-2W-0.5Y_2O_3) alloy. Mater. Sci. & Eng. A 2011; 528; 13-14; 4579-4584
[8] Schaeublin R, Leguey T, Spätig P, Baluc N, Victoria M. Microstructure and mechanical properties of two ODS ferritic/martensitic steels. J. Nucl. Mater. 2002; 307-311: 778-782
[9] Sagaradze VV, Shalaev VI, Arbuzov VL, Goshchitskii BN, Tian Y, Qun W, Jiguang S. Radiation resistance and thermal creep of ODS ferritic steels. J. Nucl. Mater. 2001; 295: 265-272
[10] Klimenkov M., Möslang A., Materna-Morris E. Helium influence on the microstructure and swelling of 9%Cr ferritic steel after neutron irradiation to 16.3 dpa. J. Nucl. Mater. 2014; 1-3: 54-59
[11] Chen T, Aydogan E, Gigax JG, Chen D, Wang J, Wang X, Ukai S, Garner FA, Shao L. Microstructural changes and void swelling of a 12Cr ODS ferritic-martensitic alloy after high-dpa self-ion irradiation. J. Nucl. Mater. 2015; 467:42-49
[12] Brodrick J, Hepburn DJ, Ackland GJ. Mechanism for radiation damage resistance in yttrium oxide dispersion strnegthened steels. J. Nucl. Mater. 2014; 445: 291-297
[13] Karak SK, Chudoba T, Witczak Z, Lojkowski W, Manna I. Development of ultra high strength nano-Y_2O_3 dispersed ferritic steel by mechanical alloying and hot isostatic pressing. Mater. Sci. & Eng. A 2011; 528: 7475-7483
[14] Muroga T, Nagasaka T, Li Y, Abe H, Ukai S, Kimura A, Okuda T. Fabrication and characterization of reference 9Cr and 12Cr-ODS low activation ferritic/martensitic steels. Fus. Eng. & Des. 2014; 89; 7-8: 1717-1722
[15] De Castro V, Leguey T, Monge MA, Muñoz A, Pareja R, Amador DR, Torralba JM, Victoria M: Mechanical dispersion of Y_2O_3 nanoparticles in steel EUROFER 97: Process and optimization. J. Nucl. Mater. 2003; 322; 2-3:228-234
[16] Alinger MJ, Odette GR, Hoelzer DT. The development and stability of Y-Ti-O nanoclusters in mechanically alloyed Fe-Cr based ferritic alloys. J. Nucl. Mater. 2004; 329-333: 382-386
[17] Arkhurst BM, Park J-J, Lee CH, Kim JH. Direct laser deposition of 14Cr oxide dispersion strengthened steel powders using Y_2O_3 and HfO_2 dispersoids. Korean J. Met. Mater. 2017; 55; 8: 550-558
[18] Walker JC, Berggreen KM, Jones AR, Sutcliffe CJ. Fabrication of Fe-Cr-Al oxide dispersion strengthened PM2000 alloy using selective laser melting. Adv. Eng. Mater. 2009; 11; 541-546
[19] Boegelein T, Dryepondt SN, Pandey A, Dawson K, Tatlock GJ. Mechanical response and deformation mechanisms of ferritic oxide dispersion strengthened steel structures produced by selective laser melting. Acta. Mater. 2015; 87: 201-215
[20] Boegelein T, Louvis E, Dawson K, Tatlock GJ, Jones AR. Characterisation of a complex thin walled structure fabricated by selective laser melting using a ferritic oxide dispersion strengthened steel. Mater. Charact. 2016; 112:30-40
[21] Streubel R, Wilms MB, Doñate-Buendia C, Weisheit A, Barcikowski S, Schleifenbaum JH, Gökce B. Depositing laser-generated nanoparticles

on powders for additive manufacturing of oxide dispersion strengthened alloy parts via laser metal deposition. Japanese J. Appl. Phys. 2018; 57

[22] Doñate-Buendía C., Frömel F., Wilms M. B., Streubel R., Tenkamp J., Hupfeld T., Nachev M., Gökce E., Weisheit A., Barcikowski S., Walther F., Schleifenbaum J. H., Gökce B. Mat & Des. 154, 2018, 360-369

[23] Zhang D., Gökce B., Barcikowski S. Laser Synthesis and Processing of Colloids – Fundamentals and Applications. Chem. Rev., 2017, 117, 3990

[24] Schmitz T., Wiedwald U., Dubs C., Gökce B. Ultrasmall Yttrium Iron Garnet Nanoparticles with High Coercivity at Low Temperature Synthesized by Laser Ablation and Fragmentation of Pressed Powders. Chem. Phys. Chem. 2017, 18, 1125

[25] Zhang D., Lau M., Lu S., Barcikowski S., Gökce B. Germanium Sub-Microspheres Synthesized by Picosecond Pulsed Laser Melting in Liquids: Educt Size Effects. Sci. Rep., 2017, 7, 40355

[26] Waag F., Gökce B., Kalapu C., Bendt G., Salamon S., Landers J., Hagemann U., Heidelmann M., Schulz S., Wende H., Hartmann N., Behrens M., Barcikowski S. Adjusting the catalytic properties of cobalt ferrite nanoparticles by pulsed laser fragmentation in water with defined energy dose. Sci Rep, 2017, 7, 1316